energies

MDPI

Article

Inverse Open Circuit Voltage Curve Model for $LiCoO_2$ Battery at Different Temperatures

Simone Barcellona [1,*], Lorenzo Codecasa [1] and Silvia Colnago [2]

[1] Department of Electronics, Information and Bioengineering, Politecnico di Milano, 20133 Milan, Italy; lorenzo.codecasa@polimi.it
[2] Department of Generation Technologies and Materials, Ricerca sul Sistema Energetico S.p.A., 20134 Milan, Italy; silvia.colnago@rse-web.it
* Correspondence: simone.barcellona@polimi.it

Abstract: Lithium-ion batteries are widely used in a variety of applications. For effective battery management, accurate estimation of the state of charge (SOC) is essential. One of the most commonly employed methods for SOC estimation relies on the open circuit voltage (OCV) curve with respect to SOC. However, inverting the OCV-SOC function is not always straightforward. This paper proposes a novel analytical function that directly models the inverse OCV-SOC function, providing a more efficient and reliable method for SOC estimation. Moreover, the dependency of the proposed function on battery temperature is also being investigated, allowing for a wider application of the method under different OCV measuring conditions.

Keywords: lithium-ion batteries; open circuit voltage characteristics; cycle aging

Citation: Barcellona, S.; Codecasa, L.; Colnago, S. Inverse Open Circuit Voltage Curve Model for $LiCoO_2$ Battery at Different Temperatures. *Energies* **2024**, *17*, 5137. https://doi.org/10.3390/en17205137

Academic Editor: Carlos M. Costa

Received: 17 September 2024
Revised: 11 October 2024
Accepted: 14 October 2024
Published: 16 October 2024

1. Introduction

Lithium-ion batteries (LiBs) are a highly popular research topic that attracts interest from scientists across various fields. This widespread interest is driven by the fact that LiBs are integral to numerous applications, and virtually everyone owns at least one device powered by them. LiBs are found in small electronic devices such as smartphones and notebooks, as well as in larger applications like electric vehicles (EVs) [1,2]. Additionally, LiBs are used as energy storage solutions supporting renewable energy sources like solar and wind, thus facilitating the transition to a more sustainable energy grid [3]. Governments are also offering incentives to promote the study of LiBs due to their potential to address environmental pollution and the energy crisis. Specifically, EVs, which rely on LiBs, are becoming increasingly popular as a means to reduce carbon emissions and dependence on fossil fuels.

The reason why LiBs are among the most widely used energy storage systems is their ability to offer high energy and power density while being efficient and having very low self-discharge with no memory effect. Additionally, LiBs generally have a long lifespan, which varies depending on the type of battery and its usage [4,5]. Accurate estimation of the state of charge (SOC) is crucial for effective LiB management. Without precise SOC estimation, it is challenging to ensure that the battery operates within its optimal and safe limits. Furthermore, SOC estimation provides users with valuable information on how long the battery can be used before requiring recharging [6].

The SOC estimation can be performed either online or offline [7]. Among the various methods, the well-known coulomb counting method is considered the gold standard due to its simplicity. This method requires merely integrating the battery current during its usage. Unfortunately, this simplicity is offset by a major drawback: it necessitates a highly accurate current sensor to prevent noise, which, over the integration period, can result in significant errors [8]. Additionally, SOC estimation can be affected by changes in temperature or aging, which alters the battery capacity. SOC is calculated by integrating the current to obtain the

actual ampere-hours extracted from a fully charged battery, divided by the total amount of ampere-hours that can be extracted, i.e., the battery capacity. Since the latter can change reversibly or irreversibly due to temperature or aging, correct SOC estimation requires knowledge of the actual battery capacity.

Another SOC estimation method relies on the open circuit voltage (OCV) curve, which relates the OCV to the SOC or the absolute state of discharge (SOD) of a battery [9,10]. Unlike coulomb counting, this method is highly precise, but its main drawback is that acquiring an OCV point requires the battery to be at rest for a sufficient period [11]. Consequently, this method cannot be used online. However, it can be employed to support and correct the coulomb counting or used in model-based estimation methods where the OCV can be estimated online by the battery model embedded in the battery management system (BMS), allowing the SOC to be determined. In the latter case, the accuracy of the online SOC estimation depends on the precision of the model, specifically on the parameter estimation [12,13].

In the literature, both table-based methods and numerous analytical functions have been proposed to model the OCV-SOC relationship. The former methods are simple and demand very low computational resources, but they require significant memory to store a large number of experimental data points, which are not always readily available [14]. Analytical functions, on the other hand, can require significant computational resources depending on the type of function and the number of parameters involved. However, they can be derived from a small number of experimental points. A good review of analytical functions can be found in [10]. Specifically, they can be implemented using polynomial expressions of different degrees or other transcendental functions such as exponential and logarithmic forms [15–18]. The combination of different expressions can provide a good trade-off between accuracy and simplicity [8,10,19].

As with coulomb counting, the OCV-SOC relationship can change with aging and temperature. Therefore, it is crucial not only to model the OCV-SOC curve for specific aging and temperature conditions but also to consider how this relationship varies with changes in these factors. In the literature, several studies have examined and modeled the variation of the OCV-SOC curve with aging or temperature. For instance, the authors in [20] adjusted the SOC using the actual value of the battery capacity, resulting in nearly coincident OCV-SOC curves across various aging levels. Similarly, in [21], the authors obtained the OCV-SOC curves at different aging conditions by adding an appropriate value to the OCV-SOC relationship of the fresh battery. Meanwhile, in [22], another study utilized both coulomb-counting-based SOC estimation and the relationship between aging level and SOC, as determined from the OCV curve. The researchers in [23] investigated the impact of temperature using a lookup table to address the OCV-SOC curve changes with temperature. An alternative strategy was employed in [24], where a temperature correction factor was implemented to improve the model's adaptability to temperature variations. Additionally in [25], a function was proposed to compensate for capacity variations and, consequently, the OCV curve changes caused by temperature shifts. In [26], the authors proposed an analytical function based on a double exponential term to model the OCV as a function of the absolute SOD. They considered the temperature effect by analyzing how the parameters of that model varied with battery temperature.

However, all the aforementioned analytical functions model the OCV as a function of SOC, or absolute SOD. Nevertheless, we are often more interested in determining the SOC from a given OCV measurement. A significant challenge arises when attempting to invert the OCV-SOC functions. When the direct OCV-SOC relationship is simple, it may be possible to analytically invert the function. The simplest invertible OCV-SOC model is the Unnewehr model [27] and the piece-wise Unnewerh model [28]. The primary benefit of such inversion is that it results in an inverted SOC-OCV model that utilizes the same set of parameters as the direct OCV-SOC model. However, the accuracy of the inverted SOC-OCV model depends on the precision of the direct OCV-SOC model and the specific conditions under which it was developed. On the other hand, for more complex

OCV-SOC analytical functions, this inversion requires numerical methods, which can be computationally intensive and time-consuming, particularly for real-time BMSs [29]. To overcome these issues, it could be preferable to directly construct inverted SOC-OCV analytical functions, which provide several advantages, including easier SOC prediction and streamlined error analysis during estimation. An example is provided in [30], where the authors proposed an improved coulomb counting method based on a piecewise-linear inverted SOC-OCV function for SOC estimation. However, to the best of the authors' knowledge, no other studies have explored the possibility of using these inverted functions or their variations with temperature.

In light of the above, in this work, we proposed a novel analytical function that directly models the inverse relationship, allowing for the estimation of SOC from OCV without the need for numerical inversion. This approach not only simplifies the computational process but also enhances the efficiency and reliability of SOC estimation. Our proposed model aims to provide a more practical solution for real-time applications, where quick and accurate SOC determination is essential. In this study, the focus was on modeling the discharge OCV curve, and instead of using SOC, we opted to use absolute SOC, q. To achieve this, an analytical expression with only two Gaussian terms was proposed and analyzed. The dependency of its parameters on battery temperature was also studied to develop a temperature-dependent model. Moreover, the proposed procedure is designed to be valid for a fixed state of health of the battery. This means that the battery could either be a fresh cell or an aged one, as in the case of second-life batteries. Specifically, an aged battery may exhibit changes in both actual capacity and internal resistance, which are the two primary indicators used to assess the state of health. Finally, the proposed model was validated through an extensive experimental campaign.

2. Battery Model

To obtain the discharge OCV curve, the output battery voltage must match the equilibrium voltage, i.e., the OCV. This is only observable when the battery current is zero and all relaxation transients have extinguished. To achieve this, as suggested in the literature, one can use the well-known galvanostatic intermittent titration technique (GITT), in which the battery undergoes partial discharges followed by an appropriate relaxation period [31], or the pseudo-OCV test, where the battery is continuously discharged at a very low current rate (<0.1C) to minimize overpotentials [32]. However, both methods are time-consuming.

For the analysis carried out in the present paper, it was necessary to obtain OCV curves at different temperatures, and there was a risk of accelerating some aging mechanisms during the characterization process, particularly at high and low temperatures. To address this, it was chosen to perform the OCV curve by discharging the battery at 1C, which expedited the procedure at different temperatures. Of course, using this method means that it is not possible to neglect the overpotentials within the battery, resulting in the OCV differing from the measured output battery voltage due to these overpotentials. The latter arise from various phenomena within the battery, such as voltage drops across the ohmic resistance, the solid electrolyte interface (SEI) film, and diffusion-related overpotentials. Therefore, the discharge voltage curves must be corrected by calculating and eliminating these contributions.

To accomplish this, we can refer to the electric battery model illustrated in Figure 1. This model consists of several lumped elements: a q-controlled voltage source, $v_{eq}(q)$, which represents the OCV as a function of the absolute SOC, q, and is connected in series with various RC elements that model different battery phenomena. The first element is the series resistor, R_Ω, which models the ohmic resistance of the electrodes, current collectors, and electrolyte. The second element is a parallel RC branch composed of the resistor, R_{film}, and a capacitor, C_{film}, representing the resistance and capacitance of the SEI film. The third element is a parallel RC branch modeling the charge transfer resistance, R_{ct}, and double-layer capacitance, C_{dl}. The final component is a parallel RC branch that models the

diffusion phenomena of lithium\lithium-ion within the electrodes\electrolyte, represented by the resistor R_{dif} and capacitor C_{dif}. The equation governing this electrical circuit model is:

$$v_{eq} = v_{out} - R_{\Omega} i - v_{film} - v_{ct} - v_{dif}. \quad (1)$$

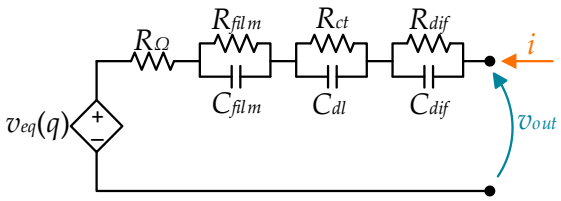

Figure 1. Electric circuit battery model.

To eliminate the contributions from battery overpotentials, it is possible to consider that when the battery begins discharging at a 1C current rate, the electrical transient caused by the various phenomena (modeled by the different parallel RC branches) occurs. After a suitable time interval, the battery can be considered to be in a steady-state condition, where the capacitors can be treated as open circuits, and (1) becomes:

$$v_{eq} = v_{out} - R_{\Omega} i - R_{film} i - R_{ct} i - R_{dif} i. \quad (2)$$

In this state, all resistance contributions can be summed, and the total voltage drop across these resistors, related to the battery overpotentials, can be eliminated following the procedure outlined in [33]. This approach assumes that the total battery resistance remains relatively constant with SOC. While this resistance typically varies with SOC, at temperatures above 15 °C, the change is minimal [34], especially between 20% and 100% of SOC, where it remains nearly constant, even under different cycling levels [35]. Then, the q-OCV curve was obtained, and the section of this curve corresponding to that time interval was eliminated.

The absolute SOC, q, is defined as follows:

$$q(t) = \frac{1}{3600} \int_0^t i \cdot d\tau + q(0) \quad (3)$$

where $q(0)$ is the initial value of the absolute SOC. Thus, the SOC (expressed in percentage) can be obtained from the absolute SOC by dividing it by the actual battery capacity, C_a, as follows:

$$\text{SOC} = \frac{q}{C_a} \cdot 100. \quad (4)$$

The q-OCV curve modeling the relationship between the absolute SOC and OCV, as proposed in the present study, was developed using the following double Gaussian function:

$$q(v_{eq}) = a_1 \cdot e^{-\frac{(v_{eq}-b_1)^2}{c_1^2}} + a_2 \cdot e^{-\frac{(v_{eq}-b_2)^2}{c_2^2}} \quad (5)$$

where a_1, a_2, b_1, b_2, c_1, and c_2 are the model parameters specific to LiB. These parameters will be determined and analyzed as a function of battery temperature later in this study.

3. Test Procedure and Setup

In this work, the experimental data used are those obtained from [26] related to a lithium-ion pouch cell with a carbon-based anode and a lithium–cobalt-oxide cathode ($LiCoO_2$), model 8773160K (10 Ah, 2.75–4.2 V, LxWxH: 152 × 72 × 9 mm), manufactured by General Electronics Battery Co., Ltd (Shenzhen, China). For completeness, the experimental setup and procedure are also detailed here.

3.1. Experimental Setup

The discharge OCV curves were obtained testing the LiB cell using the setup shown in Figure 2, which comprised a potentiostat (SP-150) and a 100 A booster (VMP3B-100) from Biologic Science Instruments (Seyssinet-Pariset, France). These devices were operated via EC-Lab (v11.34) software on a PC connected to the SP-150 via an Ethernet cable.

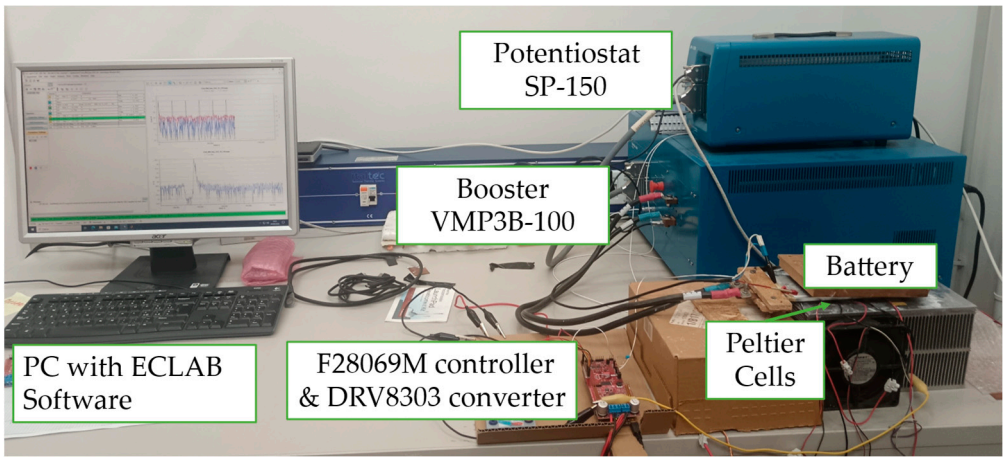

Figure 2. Overview of the experimental setup.

Usually, battery temperature is controlled using a climate chamber. However, this method can lead to variations in battery temperature during discharge due to self-heating. To address this issue, as done in [35–37], the battery temperature was regulated in an open space using three Peltier cells positioned beneath the battery cell. The opposite side of the Peltier cells was mounted on a heatsink equipped with two fans.

To optimize heat transfer, thermal paste was applied between the Peltier cells and the battery bottom face, while the top face was left exposed to the air. This setup allowed the Peltier cells, when properly controlled, to maintain a consistent and uniform battery temperature throughout the discharge process. Although temperature control was applied only to the bottom side of the battery and the temperature was measured at the center of the top side, the temperature gradient across the battery cell was minimal due to its thin profile, as shown in Figure 3, and was therefore neglected.

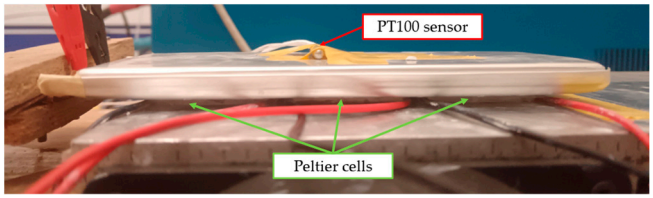

Figure 3. Zoom of the battery under test.

The Peltier cells, model TEC1-12706 (12 V, 6 A), were connected in series, and their current was controlled by a Texas Instruments DRV8303 full-bridge converter, managed by an F28069M controller board featuring a proportional-integral (PI) regulator. The converter was powered by a DC voltage source, while a PT100 sensor positioned on the top face of the battery monitored the temperature, providing feedback to the F28069M controller board. The acquired battery temperature (T_{meas}) was compared with the reference temperature (T_{ref}), and the resulting error was fed into the PI regulator. The PI regulator, in turn, adjusted the duty cycle that drives the converter. Notably, since the converter utilizes a full-bridge topology, the current in the Peltier cells can flow in both directions, allowing the cells to either cool or heat the battery as needed. The scheme of temperature control is reported in Figure 4.

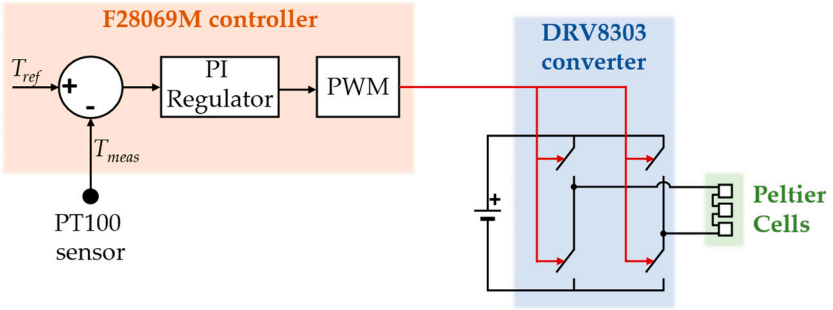

Figure 4. Temperature control scheme.

3.2. Test Procedure

The output battery voltage profiles were obtained for different fixed battery temperatures ranging from 10 °C to 50 °C, with 5 °C intervals. For each temperature setting, the LiB cell was initially fully charged using a constant current, constant voltage (CC-CV) protocol and then discharged following a CC protocol.

Specifically, during the charging phase, a constant current of 10 A (1C) was used until the LiB cell reached the maximum cut-off voltage of 4.2 V. The charging continued with a constant voltage until the battery current decreased to below 200 mA (0.02C), indicating that the LiB cell was fully charged at 100% of SOC. Subsequently, during the discharging phase, a constant current of 10 A (1C) was applied until the LiB cell reached the minimum cut-off voltage of 2.75 V.

4. Proposed Model Characterization

To characterize the proposed OCV model for the pouch $LiCoO_2$ battery cell under test, nine discharge voltage curves were obtained at temperatures of 10, 15, 20, 25, 30, 35, 40, 45, and 50 °C. Figure 5 illustrates the experimental discharge profiles along with the corresponding battery temperature measurements, as obtained using the procedure described in the previous section.

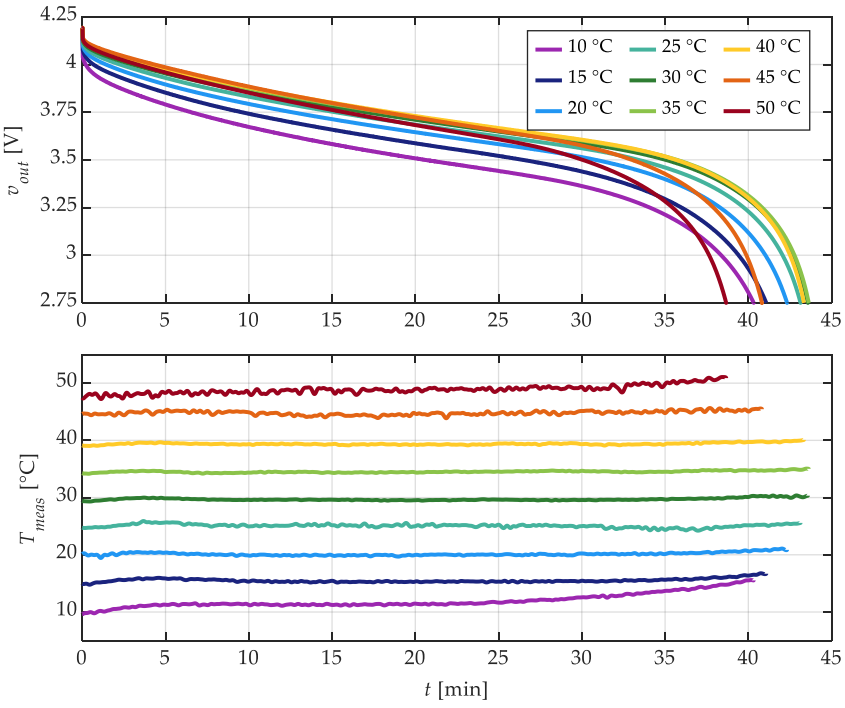

Figure 5. Experimental discharge voltage curves and related battery temperatures.

As discussed in Section 2, these voltage profiles differ from the OCV profiles due to the internal voltage drop. The latter was estimated and removed according to the procedure described in [33], where the time interval corresponding to the electrical transient was calculated for each discharge curve by considering a voltage derivative of 1 mV/s. Similarly, the related segment of the OCV curve was removed.

Although the battery temperature control system is designed to maintain the temperature constant at the set value, slight variations can occur due to self-heating and the system's capacity to keep the reference temperature stable. Therefore, the average battery temperature, T, during discharge was used.

The proposed q-OCV model (5) includes six parameters that need to be determined. To accomplish this, the nonlinear least squares method was employed using the "fit" function in Matlab (2022b) software. Figure 6 presents a comparison between the experimental and modeled q-OCV curves at different battery temperatures, illustrating the effectiveness of the proposed model. Additionally, the corresponding coefficients of determination (R^2) were calculated and are shown in Figure 7 as a global indicator of the goodness of fit. These coefficients are all greater than 0.9981 for every q-OCV test.

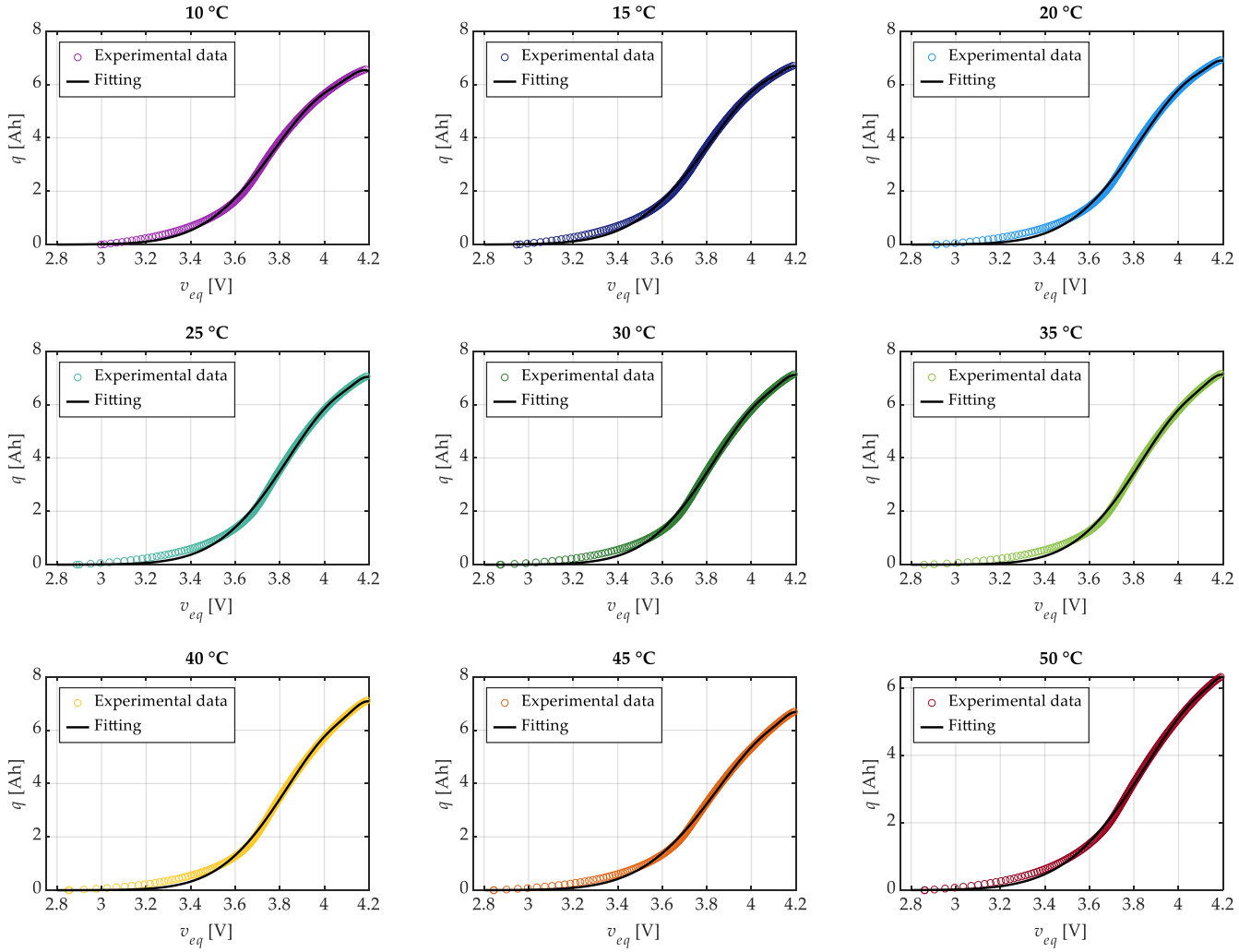

Figure 6. Comparison between the experimental and modeled discharge q-OCV curves (with all six parameters free).

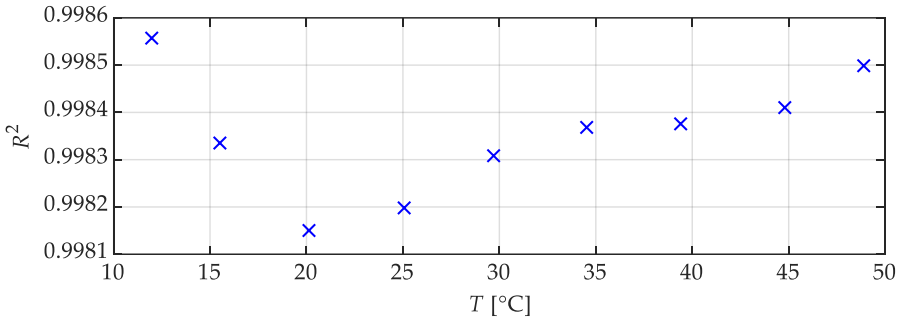

Figure 7. Coefficient of determination for the discharge q-OCV fitting with all six parameters free.

Figure 6 shows that the battery under test exhibited a capacity lower than the nominal value (10 Ah) at the reference temperature of 25 °C, due to prior usage and prolonged storage before testing. However, this does not affect the analysis, as the proposed procedure is intended to be valid for a fixed state of health and is likely applicable even when considering second-life batteries.

The six parameters of the proposed q-OCV model (5) for different battery temperatures are shown in Figure 8. This figure highlights how these parameters vary with battery temperature. If it is possible to derive simple analytical expressions to model these trends, a temperature-dependent q-OCV model can be developed. It is worth noting that the trends of the six parameters are not well defined but quite similar, suggesting there may be fewer degrees of freedom than initially expected.

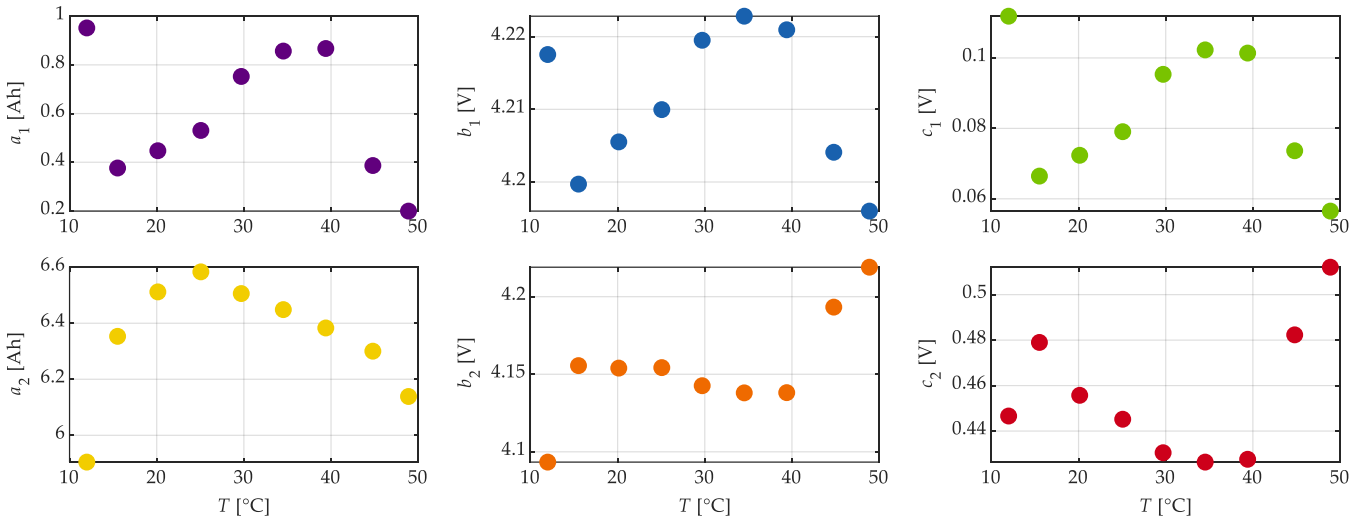

Figure 8. Trend of the six parameters in the proposed discharge q-OCV model.

Following the approach in [26], and after various trials, we found that by fixing the parameters a_1, b_1, c_1, and c_2 in model (5) to their average value obtained from the previous fitting (a_1 = 0.5964 Ah, b_1 = 4.211 V, c_1 = 0.08433 V, c_2 = 0.4561 V), it was possible to refit the model with only two free parameters (a_2 and b_2) while still achieving good results. As shown in Figure 9, this new fitting approach maintained a strong match between the experimental and modeled q-OCV curves. The R^2 values reported in Figure 10, all greater than 0.9974, confirm the effectiveness of this approach.

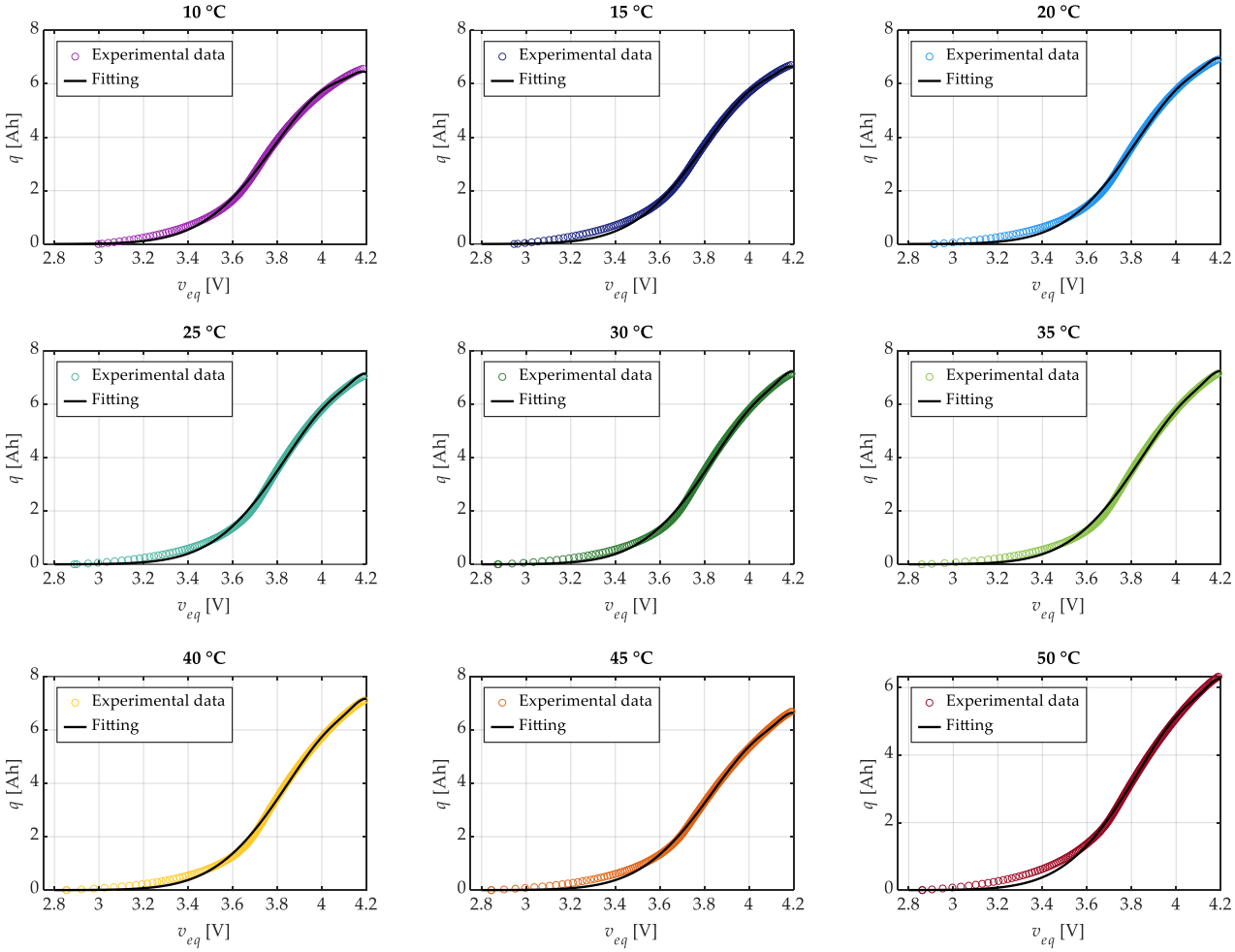

Figure 9. Comparison between the experimental and modeled discharge q-OCV curves (with just two parameters free).

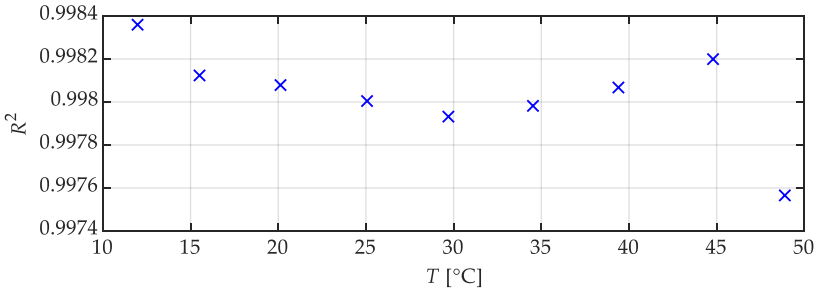

Figure 10. Coefficient of determination for the discharge q-OCV fitting with just two parameters free.

Finally, Figure 11 illustrates the trend of the two parameters, a_2 and b_2, as functions of battery temperature, along with their corresponding fitting functions. From this figure, it is evident that the trends of the two parameters are more defined compared to the previous case, suggesting parabolic behavior. Therefore, they could be fitted using the following polynomial functions:

$$\begin{aligned} a_2 &= -5.078 \cdot 10^{-5} \cdot T^3 + 2.246 \cdot 10^{-3} \cdot T^2 + 1.207 \cdot 10^{-2} \cdot T + 5.687 \\ b_2 &= -1.196 \cdot 10^{-4} \cdot T^2 + 8.328 \cdot 10^{-3} \cdot T + 4.029 \end{aligned} \tag{6}$$

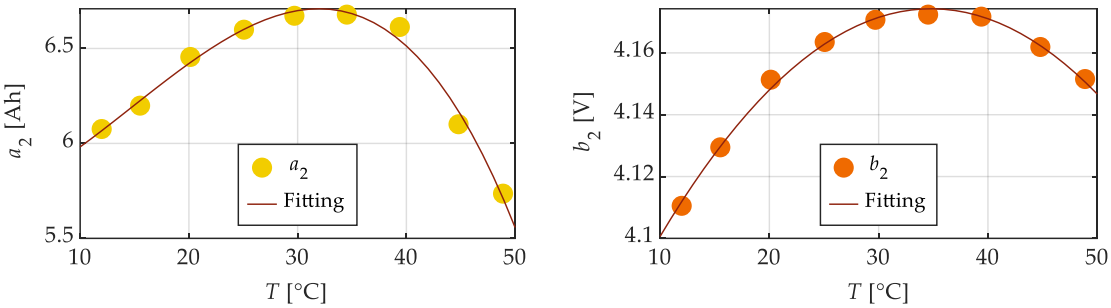

Figure 11. Trend of the parameters a_2 and b_2 in the proposed discharge q-OCV model with the other parameters fixed.

5. Proposed SOC Estimation

Through the q-OCV model developed in the previous section, the SOC can be estimated. To achieve this, given an experimental OCV value at a specific battery temperature, T, the estimated absolute SOC, q_*, and the actual battery capacity, $C_{a,*}$, can be directly obtained using Equation (5). Specifically, the latter can be calculated by imposing the maximum cut-off voltage of 4.2 V in (5). Finally, the estimated SOC_* is derived using Equation (4).

To assess the accuracy of the SOC estimation, its deviation was calculated as follows:

$$\mathrm{SOC}_{\mathrm{dev}} = |\mathrm{SOC}_* - \mathrm{SOC}| \tag{7}$$

where SOC_* and SOC represent the estimated and experimental SOC of the battery, respectively. The experimental SOC is still derived using (4), but the absolute SOC, q, and the actual battery capacity, C_a, are obtained experimentally by integrating the battery current.

Figure 12 illustrates the SOC estimation deviations, expressed as percentages, across the entire voltage range for different temperatures, while Figure 13 highlights the mean and maximum values of these deviations, also expressed as percentages, calculated across the entire voltage range for different temperatures. From this figure, it is evident that the proposed estimation method is quite accurate. The mean SOC deviation is less than 1.5% for all temperatures, and the maximum deviation is under 4%.

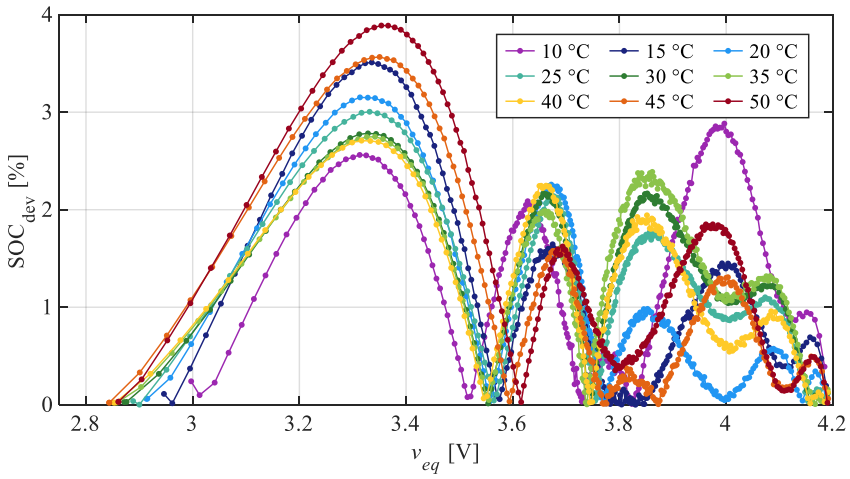

Figure 12. SOC estimation deviation across different temperatures.

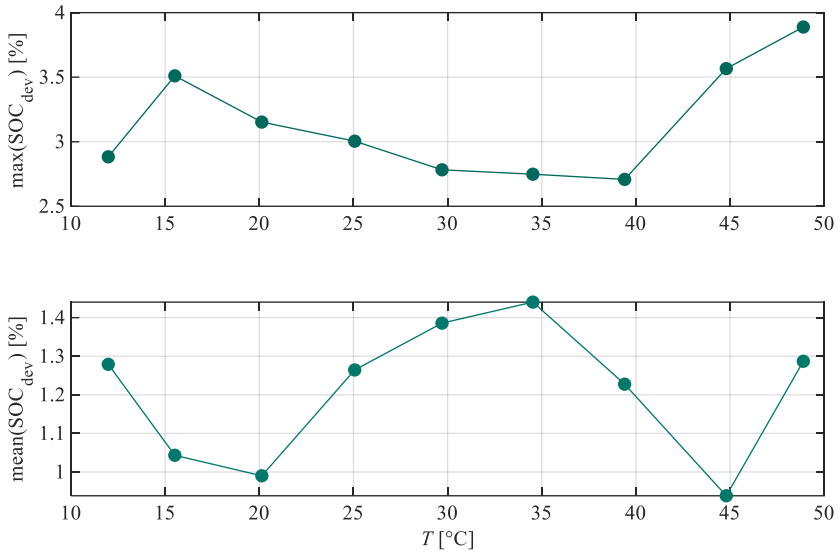

Figure 13. Maximum and mean values of SOC estimation deviation across different temperatures.

6. Conclusions

In this paper, a novel analytical function was proposed to model the inverse OCV-SOC relationship, enabling SOC estimation from OCV without the need for numerical inversion. For this analysis, the absolute state of charge, q, expressed in Ah, was used instead of the traditional SOC.

The proposed q-OCV curve model is based on a double Gaussian function with six parameters to be fitted. This model was analyzed for a $LiCoO_2$ battery tested at nine different temperatures, ranging from 10 °C to 50 °C.

Initially, the nonlinear least squares method was applied to fit the experimental curves to the model, identifying the six parameters for all tested temperatures. Subsequently, four parameters (a_1, b_1, c_1, and c_2) were fixed at their average values, and the fitting process was repeated with only two parameters (a_2 and b_2) left free. Finally, these two parameters were expressed as functions of temperature, completing the full model.

The proposed model was validated across different temperatures by estimating SOC from experimental OCV values. It demonstrated high accuracy, with a mean SOC deviation of less than 1.5% and a maximum deviation of less than 4%. This model offers reliable and precise SOC estimation, making it highly applicable across a range of use cases.

Author Contributions: Conceptualization, S.B. and S.C.; methodology, S.B. and S.C.; validation, S.B. and S.C.; formal analysis, S.B. and S.C.; writing—original draft preparation, S.B. and S.C.; writing—review and editing, S.B., L.C., and S.C.; supervision, L.C. All authors have read and agreed to the published version of the manuscript.

Funding: The work of Silvia Colnago has been financed by the Research Fund for the Italian Electrical System under the Three-Year Research Plan 2022–2024 (DM MITE No. 337, 15 September 2022), in compliance with the Decree of 16 April 2018.

Data Availability Statement: The author elects to not share data.

Acknowledgments: We would like to acknowledge the use of ChatGPT-3.5 (OpenAI, https://chat.openai.com/) for proofreading our final draft.

Conflicts of Interest: Author Silvia Colnago was employed by the company Ricerca sul Sistema Energetico S.p.A. Silvia Colnago and the remaining authors declare that the research was conducted in the absence of any commercial or financial relationships that could be construed as a potential conflict of interest.

References

1. Duh, Y.-S.; Lin, K.H.; Kao, C.-S. Experimental Investigation and Visualization on Thermal Runaway of Hard Prismatic Lithium-Ion Batteries Used in Smart Phones. *J. Therm. Anal. Calorim.* **2018**, *132*, 1677–1692. [CrossRef]
2. Chen, W.; Liang, J.; Yang, Z.; Li, G. A Review of Lithium-Ion Battery for Electric Vehicle Applications and Beyond. *Energy Procedia* **2019**, *158*, 4363–4368. [CrossRef]
3. Blomgren, G.E. The Development and Future of Lithium Ion Batteries. *J. Electrochem. Soc.* **2017**, *164*, A5019–A5025. [CrossRef]
4. Mahmoudzadeh Andwari, A.; Pesiridis, A.; Rajoo, S.; Martinez-Botas, R.; Esfahanian, V. A Review of Battery Electric Vehicle Technology and Readiness Levels. *Renew. Sustain. Energy Rev.* **2017**, *78*, 414–430. [CrossRef]
5. Tie, S.F.; Tan, C.W. A Review of Energy Sources and Energy Management System in Electric Vehicles. *Renew. Sustain. Energy Rev.* **2013**, *20*, 82–102. [CrossRef]
6. Singh, A.; Pal, K.; Vishwakarma, C.B. State of Charge Estimation Techniques of Li-Ion Battery of Electric Vehicles. *e-Prime—Adv. Electr. Eng. Electron. Energy* **2023**, *6*, 100328. [CrossRef]
7. Zhou, W.; Zheng, Y.; Pan, Z.; Lu, Q. Review on the Battery Model and SOC Estimation Method. *Processes* **2021**, *9*, 1685. [CrossRef]
8. Zhang, C.; Jiang, J.; Zhang, L.; Liu, S.; Wang, L.; Loh, P. A Generalized SOC-OCV Model for Lithium-Ion Batteries and the SOC Estimation for LNMCO Battery. *Energies* **2016**, *9*, 900. [CrossRef]
9. Baccouche, I.; Jemmali, S.; Manai, B.; Omar, N.; Amara, N. Improved OCV Model of a Li-Ion NMC Battery for Online SOC Estimation Using the Extended Kalman Filter. *Energies* **2017**, *10*, 764. [CrossRef]
10. Weng, C.; Sun, J.; Peng, H. A Unified Open-Circuit-Voltage Model of Lithium-Ion Batteries for State-of-Charge Estimation and State-of-Health Monitoring. *J. Power Sources* **2014**, *258*, 228–237. [CrossRef]
11. Lee, S.; Kim, J.; Lee, J.; Cho, B.H. State-of-Charge and Capacity Estimation of Lithium-Ion Battery Using a New Open-Circuit Voltage versus State-of-Charge. *J. Power Sources* **2008**, *185*, 1367–1373. [CrossRef]
12. Li, J.; Wang, L.; Lyu, C.; Pecht, M. State of Charge Estimation Based on a Simplified Electrochemical Model for a Single $LiCoO_2$ Battery and Battery Pack. *Energy* **2017**, *133*, 572–583. [CrossRef]
13. Li, J.; Lai, Q.; Wang, L.; Lyu, C.; Wang, H. A Method for SOC Estimation Based on Simplified Mechanistic Model for $LiFePO_4$ Battery. *Energy* **2016**, *114*, 1266–1276. [CrossRef]
14. Sundaresan, S.; Devabattini, B.; Kumar, P.; Pattipati, K.; Balasingam, B. Tabular Open Circuit Voltage Modelling of Li-Ion Batteries for Robust SOC Estimation. *Energies* **2022**, *15*, 9142. [CrossRef]
15. Sun, D.; Yu, X.; Wang, C.; Zhang, C.; Huang, R.; Zhou, Q.; Amietszajew, T.; Bhagat, R. State of Charge Estimation for Lithium-Ion Battery Based on an Intelligent Adaptive Extended Kalman Filter with Improved Noise Estimator. *Energy* **2021**, *214*, 119025. [CrossRef]
16. Zhao, S.; Duncan, S.R.; Howey, D.A. Observability Analysis and State Estimation of Lithium-Ion Batteries in the Presence of Sensor Biases. *IEEE Trans. Control Syst. Technol.* **2017**, *25*, 326–333. [CrossRef]
17. Xiong, R.; He, H.; Sun, F.; Zhao, K. Online Estimation of Peak Power Capability of Li-Ion Batteries in Electric Vehicles by a Hardware-in-Loop Approach. *Energies* **2012**, *5*, 1455–1469. [CrossRef]
18. Ta, K.P.; Newman, J. Proton Intercalation Hysteresis in Charging and Discharging Nickel Hydroxide Electrodes. *J. Electrochem. Soc.* **1999**, *146*, 2769–2779. [CrossRef]
19. Hu, Y.; Yurkovich, S.; Guezennec, Y.; Yurkovich, B.J. Electro-Thermal Battery Model Identification for Automotive Applications. *J. Power Sources* **2011**, *196*, 449–457. [CrossRef]
20. Wang, L.; Lu, D.; Liu, Q.; Liu, L.; Zhao, X. State of Charge Estimation for LiFePO4 Battery via Dual Extended Kalman Filter and Charging Voltage Curve. *Electrochim. Acta* **2019**, *296*, 1009–1017. [CrossRef]
21. Klintberg, A.; Klintberg, E.; Fridholm, B.; Kuusisto, H.; Wik, T. Statistical Modeling of OCV-Curves for Aged Battery Cells. *IFAC-Pap.* **2017**, *50*, 2164–2168. [CrossRef]
22. Tong, S.; Klein, M.P.; Park, J.W. On-Line Optimization of Battery Open Circuit Voltage for Improved State-of-Charge and State-of-Health Estimation. *J. Power Sources* **2015**, *293*, 416–428. [CrossRef]
23. Xing, Y.; He, W.; Pecht, M.; Tsui, K.L. State of Charge Estimation of Lithium-Ion Batteries Using the Open-Circuit Voltage at Various Ambient Temperatures. *Appl. Energy* **2014**, *113*, 106–115. [CrossRef]
24. Farmann, A.; Sauer, D.U. A Study on the Dependency of the Open-Circuit Voltage on Temperature and Actual Aging State of Lithium-Ion Batteries. *J. Power Sources* **2017**, *347*, 1–13. [CrossRef]
25. Gismero, A.; Schaltz, E.; Stroe, D.-I. Recursive State of Charge and State of Health Estimation Method for Lithium-Ion Batteries Based on Coulomb Counting and Open Circuit Voltage. *Energies* **2020**, *13*, 1811. [CrossRef]
26. Barcellona, S.; Codecasa, L.; Colnago, S. Temperature Effect on the Open Circuit Voltage of Lithium-Ion Battery. In Proceedings of the Electrimacs 2024, Castelló de la Plana, Spain, 27–31 May 2024. presented and under press, 2024.
27. Unnewehr, L.E.; Nasar, S.A. *Electric Vehicle Technology*; John Wiley & Sons: Hoboken, NJ, USA, 1982.
28. Huang, C.-S.; Chow, M.-Y. Accurate Thevenin's Circuit-Based Battery Model Parameter Identification. In Proceedings of the 2016 IEEE 25th International Symposium on Industrial Electronics (ISIE), Santa Clara, CA, USA, 8–10 June 2016; IEEE: Piscataway, NJ, USA; pp. 274–279.
29. Sunil, S.; Sundaresan, S.; Pillai, P.; Balasingam, B. Inverse Characterization of Open-Circuit Voltage for State-of-Charge Estimation of Batteries. In Proceedings of the 2023 IEEE Transportation Electrification Conference & Expo (ITEC), Detroit, MI, USA, 21 June 2023; IEEE: Piscataway, NJ, USA; pp. 1–6.

30. Baccouche, I.; Jemmali, S.; Mlayah, A.; Manai, B.; Amara, N.E. Ben Implementation of an Improved Coulomb-Counting Algorithm Based on a Piecewise SOC-OCV Relationship for SOC Estimation of Li-IonBattery. *arXiv* **2018**, arXiv:1803.10654.
31. Qiao, X.; Wang, Z.; Hou, E.; Liu, G.; Cai, Y. Online Estimation of Open Circuit Voltage Based on Extended Kalman Filter with Self-Evaluation Criterion. *Energies* **2022**, *15*, 4373. [CrossRef]
32. Zhang, K.; Xiong, R.; Li, Q.; Chen, C.; Tian, J.; Shen, W. A Novel Pseudo-Open-Circuit Voltage Modeling Method for Accurate State-of-Charge Estimation of $LiFePO_4$ Batteries. *Appl. Energy* **2023**, *347*, 121406. [CrossRef]
33. Barcellona, S.; Grillo, S.; Piegari, L. A Simple Battery Model for EV Range Prediction: Theory and Experimental Validation. In Proceedings of the 2016 International Conference on Electrical Systems for Aircraft, Railway, Ship Propulsion and Road Vehicles & International Transportation Electrification Conference (ESARS-ITEC), Toulouse, France, 2–4 November 2016; IEEE: Piscataway, NJ, USA; pp. 1–7.
34. Chen, L.; Zhang, M.; Ding, Y.; Wu, S.; Li, Y.; Liang, G.; Li, H.; Pan, H. Estimation the Internal Resistance of Lithium-Ion-Battery Using a Multi-Factor Dynamic Internal Resistance Model with an Error Compensation Strategy. *Energy Rep.* **2021**, *7*, 3050–3059. [CrossRef]
35. Barcellona, S.; Colnago, S.; Piegari, L. Aging Effect on Lithium-Ion Battery Resistance Hysteresis. *IEEE Trans. Ind. Appl.* **2023**, *59*, 4516–4527. [CrossRef]
36. Ardani, M.I.; Patel, Y.; Siddiq, A.; Offer, G.J.; Martinez-Botas, R.F. Combined Experimental and Numerical Evaluation of the Differences between Convective and Conductive Thermal Control on the Performance of a Lithium Ion Cell. *Energy* **2018**, *144*, 81–97. [CrossRef]
37. Troxler, Y.; Wu, B.; Marinescu, M.; Yufit, V.; Patel, Y.; Marquis, A.J.; Brandon, N.P.; Offer, G.J. The Effect of Thermal Gradients on the Performance of Lithium-Ion Batteries. *J. Power Sources* **2014**, *247*, 1018–1025. [CrossRef]